Using Satellite Ocean Color Data to Derive an Empirical Model for the Penetration Depth of Solar Radiation (H_p) in the Tropical Pacific Ocean

RONG-HUA ZHANG

State Key Laboratory of Satellite Ocean Environment Dynamics, Second Institute of Oceanography, State Oceanic Administration, Hangzhou, Zhejiang, China, and Earth System Science Interdisciplinary Center, University of Maryland, College Park, College Park, Maryland

DAKE CHEN AND GUIHUA WANG

State Key Laboratory of Satellite Ocean Environment Dynamics, Second Institute of Oceanography, State Oceanic Administration, Hangzhou, Zhejiang, China

(Manuscript received 11 May 2010, in final form 28 February 2011)

ABSTRACT

Satellite-based ocean color measurements indicate clear evidence for bioclimate interactions in the tropical Pacific associated with El Niño–Southern Oscillation (ENSO). Recent modeling studies have demonstrated that ocean biology can potentially affect the climate through the penetration depth of solar radiation in the upper ocean (H_p), a primary parameter in coupling biology to physics in the ocean. At present, interannual variability in H_p and its related bioclimate feedback effects have not been adequately represented in coupled ocean–atmosphere models. In this work, chlorophyll (Chl) concentration data from the Sea-viewing Wide Field-of-view Sensor (SeaWiFS), available since 1997, are used to characterize interannual H_p variability in the tropical Pacific and to quantify its relationships with physical fields, including sea surface temperature (SST) and sea level (SL). It is found that interannual H_p variability is dominated by ENSO signals, with the largest variability located in the central basin near the date line and a coherent relationship with SST. A singular value decomposition (SVD) analysis is adopted to extract interannual covariability patterns between H_p and SST during the period 1997–2007. Their close relationships are then utilized to construct an empirical anomaly model for H_p, allowing for its prognostic estimate in terms of SST anomalies without explicit involvement of a marine ecosystem model. Validation and sensitivity experiments indicate that the empirical model can reasonably well capture interannual H_p responses to SST anomalies in association with ENSO. The derived empirical H_p model offers a simple and an effective way to parameterize and represent the effects of Chl containing biomass on penetrative solar radiation in the tropical Pacific, demonstrating the dynamical implication of remotely sensed Chl data for bioclimate coupling studies. Further improvements and applications of the empirical H_p model to climate modeling are discussed.

1. Introduction

The incoming irradiance is attenuated in the upper ocean because of pure water and biogenic components, which follow an exponential decline with depth (e.g., Paulson and Simpson 1977). The penetrative solar radiation and induced heating effects on the upper layers are affected by many factors that are controlled by different processes in the climate system and the marine ecosystem. One factor is associated with ocean biology. For example, the way in which incident solar radiation is absorbed in the mixed layer and the vertical penetration down into the subsurface layers can be significantly impacted by total phytoplankton biomass and its vertical distribution. When biological activities are strong, the incoming solar irradiance attenuates strongly in the vertical, with more heating being trapped in the mixed layer. When biological activities are weak, it can penetrate deeper and directly heat subsurface layers at the expense of the reduction of a direct heating in the mixed layer. The effects of ocean biology–induced heating can be simply represented by the penetration depth of solar radiation in the upper ocean

Corresponding author address: Rong-Hua Zhang, M Square Office Building 950, 5825 University Research Court, ESSIC, University of Maryland, College Park, College Park, MD 20740.
E-mail: rzhang@essic.umd.edu

DOI: 10.1175/2011JTECHO797.1

(H_p), a field linking the climate system to the marine ecosystem (e.g., Murtugudde et al. 2002; Ballabrera-Poy et al. 2007). Through the penetration of solar radiation, the structure and changes of H_p exert a direct influence on the heat balance of the upper ocean in the equatorial Pacific (e.g., Lewis et al. 1990). The direct thermodynamic effects further act to induce dynamic responses and feedbacks in the coupled climate system of the tropical Pacific (e.g., Schneider and Zhu 1998; Miller et al. 2003; Timmermann and Jin 2002).

Over the past decade, remote sensing has led to significant advances in the physical understanding, interpretation, and modeling efforts of ocean biology–related effects on the climate system. In particular, the time series of remotely sensed ocean color data and associated products have revolutionized how the impacts of climate variability and change on ocean biology and its related bioclimate interactions can be understood and quantified both globally and regionally (e.g., McClain et al. 1998). For example, H_p can be now derived using chlorophyll content data that are available from ocean color imagery since 1997 (e.g., McClain et al. 1998). As has been shown before (e.g., Murtugudde et al. 2002; Ballabrera-Poy et al. 2007), the derived H_p field from satellite-based measurements exhibits a clear spatial and temporal structure across the tropical Pacific basin on seasonal and interannual time scales, acting to have direct influences on the heat budget in the upper ocean of the tropical Pacific. In particular, clear evidence has been found for bioclimate coupling associated with ENSO in the tropical Pacific (e.g., Chavez et al. 1998, 1999; Strutton and Chavez 2004). For instance, Chavez et al. (1999) have demonstrated how quickly and strongly biological fields act to respond to changes in physical conditions. As estimated from satellite data, dramatic fluctuations occur in chlorophyll content during ENSO evolution, with the magnitude changing by a factor of 5 during El Niño and La Niña. The interannual changes in biological heating induced by ENSO events in the equatorial Pacific can be 20%–30% as large as its mean in magnitude (Strutton and Chavez 2004). Therefore, the ocean biology–induced heating and climate feedback need to be adequately taken into account in diagnostic and modeling studies in the tropical Pacific.

Recently, there has been an increased interest in the effects of ocean biology on the climate because of their potential for modulating ENSO (e.g., Miller et al. 2003; Shell et al. 2003; Timmermann and Jin 2002; Nakamoto et al. 2006; Ballabrera-Poy et al. 2007; Zhang et al. 2009). While physical ocean–atmosphere models of diverse types can now very well simulate interannual climate variability associated with ENSO (e.g., Zebiak and Cane 1987), large uncertainties exist in representing ocean biology–related processes and bioclimate feedback in climate models (e.g., Marzeion et al. 2005; Manizza et al. 2005; Wetzel et al. 2006; Lengaigne et al. 2007; Anderson et al. 2007; Gnanadesikan and Anderson 2009; Jochum et al. 2010). In particular, there are considerable difficulties in accurately depicting the climatological mean H_p field and its interannual variability using coupled physical–biogeochemical models in the ocean. In addition, explicitly representing all of these physical and biogeochemical components in a model increases computational costs enormously. As a result, ocean biology–induced feedback effects have not been included in many coupled models used for ENSO simulations and predictions (e.g., Zebiak and Cane 1987; Barnett et al. 1993; Syu et al. 1995; Zhang et al. 2005; Zheng et al. 2007). Furthermore, the effects of ocean biology–related heating on simulations of the mean climate and its variability in the tropical Pacific are strikingly model dependent and conflicting, even in forced ocean-alone simulations (e.g., Nakamoto et al. 2001; Murtugudde et al. 2002; Sweeney et al. 2005; Löptien et al. 2009), let alone in coupled ocean–atmosphere modeling studies (e.g., Marzeion et al. 2005; Manizza et al. 2005; Wetzel et al. 2006; Lengaigne et al. 2007; Anderson et al. 2007; Zhang et al. 2009; Gnanadesikan and Anderson, 2009; Jochum et al. 2010). As has been demonstrated by these previous modeling studies, a subtle change in H_p can have significant modulating effects on the coupled climate variability in the tropical Pacific. This indicates a clear need to realistically depict the H_p field for climate modeling at seasonal and interannual time scales. Currently, the seasonal H_p climatology field can be adequately estimated from multiyear satellite data (e.g., Ballabrera-Poy et al. 2007), which can be specified in climate models; however, its interannual variability is still difficult to accurately capture using coupled physical–biogeochemical models in the ocean.

In this work, we explore an empirical approach to modeling H_p, a field that serves as a link between the climate system and the marine ecosystem. Two steps will be taken. First, as has been successfully demonstrated in the early modeling for SST (e.g., Zebiak and Cane 1987), an anomaly modeling approach will be adopted for H_p: its total field is separated into its climatological part and interannual anomaly part (relative to its seasonally varying climatology). The former can be estimated directly from multiyear satellite data; the latter can be calculated in a prognostic way as follows. Since interannual H_p anomalies in the tropical Pacific are primarily associated with ENSO, they can be determined by using statistical methods based on their coherent relationships with perturbations of a physical field [e.g., SST and sea level (SL)]. This can offer a great

advantage to the H_p modeling because, as will be seen below, the interannual anomaly of H_p and its relationships with physical fields (e.g., SST and SL) can be adequately described by statistical models in the tropical Pacific, whereas the mean H_p climatology itself can be estimated directly and accurately from multiyear satellite observations.

Next, focused on the interannual anomaly part of H_p, an empirical modeling approach is taken to depict the response of H_p to changes in the physical system. This is based on the fact that ocean biological conditions in the tropical Pacific are strongly regulated by changes in physics. Because current high-quality satellite ocean color data have provided an opportunity to depict interannual H_p variability, its relationships with physical fields (e.g., SST and SL) can be quantified. As such, a statistical feedback model is derived to capture interannual H_p variability as a response to changes in a physical system. As has been often used (e.g., Barnett et al. 1993; Syu et al. 1995; Chang et al. 2001; Zhang et al. 2005, 2006; Zhang and Busalacchi 2008, 2009), a singular value decomposition (SVD) analysis is utilized to derive an empirical model for interannual variability of H_p. Together with its climatological part that is estimated from multiyear satellite data, the total H_p field is prognostically determined, which can be utilized for representing ocean biology–induced heating effects in climate modeling.

The paper is organized as follows. Section 2 briefly describes the satellite data, followed in section 3 by an analysis of covariability patterns between interannual variations in SST and H_p using an SVD analysis technique. Section 4 deals with the SVD-based empirical model for interannual H_p variability. The evaluation of the empirical H_p model is presented in section 5. Its application is presented in section 6 to diagnose the effects of interannual H_p variability on ocean biology–related heating in the upper ocean, which is based on an output of a hybrid coupled ocean–atmosphere model simulation of the tropical Pacific. Conclusions and a discussion are given in section 7.

2. Ocean color data and the penetration depth of solar radiation (H_p)

Some satellite-derived data are used for H_p-related analyses and statistical modeling studies. For example, high-quality ocean color data, which are able to resolve biology-related signals in the ocean (e.g., McClain et al. 1998), provide an opportunity for characterizing biological variability and quantifying its coherent relationships with physical fields (e.g., SST and SL). Here we utilize Sea-viewing Wide Field-of-view Sensor (SeaWiFS) data to estimate the interannual variability of H_p. Other physical fields are also used to explore their relationships with H_p, including SST (Reynolds et al. 2002) and SL from Ocean Topography Experiment (TOPEX)/Poseidon/*Jason-1* altimetry (e.g., Nerem and Mitchum 2002).

We use the SeaWiFS chlorophyll (Chl) content data that are estimated from ocean color imagery (e.g., McClain et al. 1998). Maps of monthly Chl fields come from level-3 monthly composites, which have been available since September 1997. The 9-km-resolution maps are binned to our analysis grid of $1° \times 0.5°$ for the period of September 1997–April 2007 (Ballabrera-Poy et al. 2003); the monthly median is used as monthly climatology in order to reduce the sensitivity to the extreme El Niño and La Niña events of 1997 and 1998. Ballabrera-Poy et al. (2007) illustrated the spatial distribution of the 12-month H_p climatology.

Interannual variations in ocean biology are clearly related with ENSO. Systematic changes are evident in the patterns of satellite-derived Chl concentrations (Fig. 1). During La Niña (Fig. 1e), high Chl concentrations are observed over the tropical Pacific ($\sim$0.5 mg m^{-3}), with increased biological production in nutrient-rich waters. During El Niño (Fig. 1c), Chl concentrations decrease dramatically, with extremely low biological production in the equatorial Pacific ($\sim$0.1 mg m^{-3}). Thus, dramatic changes in the equatorial Pacific occur with ocean biology during ENSO cycles. As observed, changes in Chl concentrations can be a factor of 5 during the 1997/98 El Niño and La Niña events.

Spatiotemporal changes in biological production affect the penetration of solar radiation in the upper ocean. The spectrum of solar insolation reaching the surface of the ocean contains energy in a wide range of frequencies. Incoming irradiance is attenuated due to both pure water and biogenic components; their corresponding diffusion coefficients can be expressed as $K_w(\lambda)$ and $K_{\mathrm{Bio}}(\lambda)$, where λ is wavelength. Below the ocean surface, the penetration of solar radiation follows a Beer–Lambert law with a wavelength-dependent absorption coefficient in the ocean. As in Murtugudde et al. (2002), a single absorption coefficient can be used to account for the average attenuation over the visible band (380–700 nm), which is written as $Q_{\mathrm{sr}}(z) = \gamma \exp(-z/H_p)$, where γ is the fraction of the radiation available to penetrate to depths beyond the very first centimeters of the sea surface. Here, the inverse of the diffusion coefficient K_p is defined as H_p, the penetration depth of solar radiation in the upper ocean. Following Murtugudde et al. (2002) and Ballabrera-Poy et al. (2007), maps of H_p are calculated from the Chl concentration data using the following empirical relationship: $K_p(x, y) = K_w + a\ \mathrm{Chl}(x, y)^b$, in which $\gamma = 0.33$, $K_w = 0.027$ m^{-1}, $a = 0.0518$ m^{-1}/(mg m^{-3})^b, and $b = 0.428$ are taken.

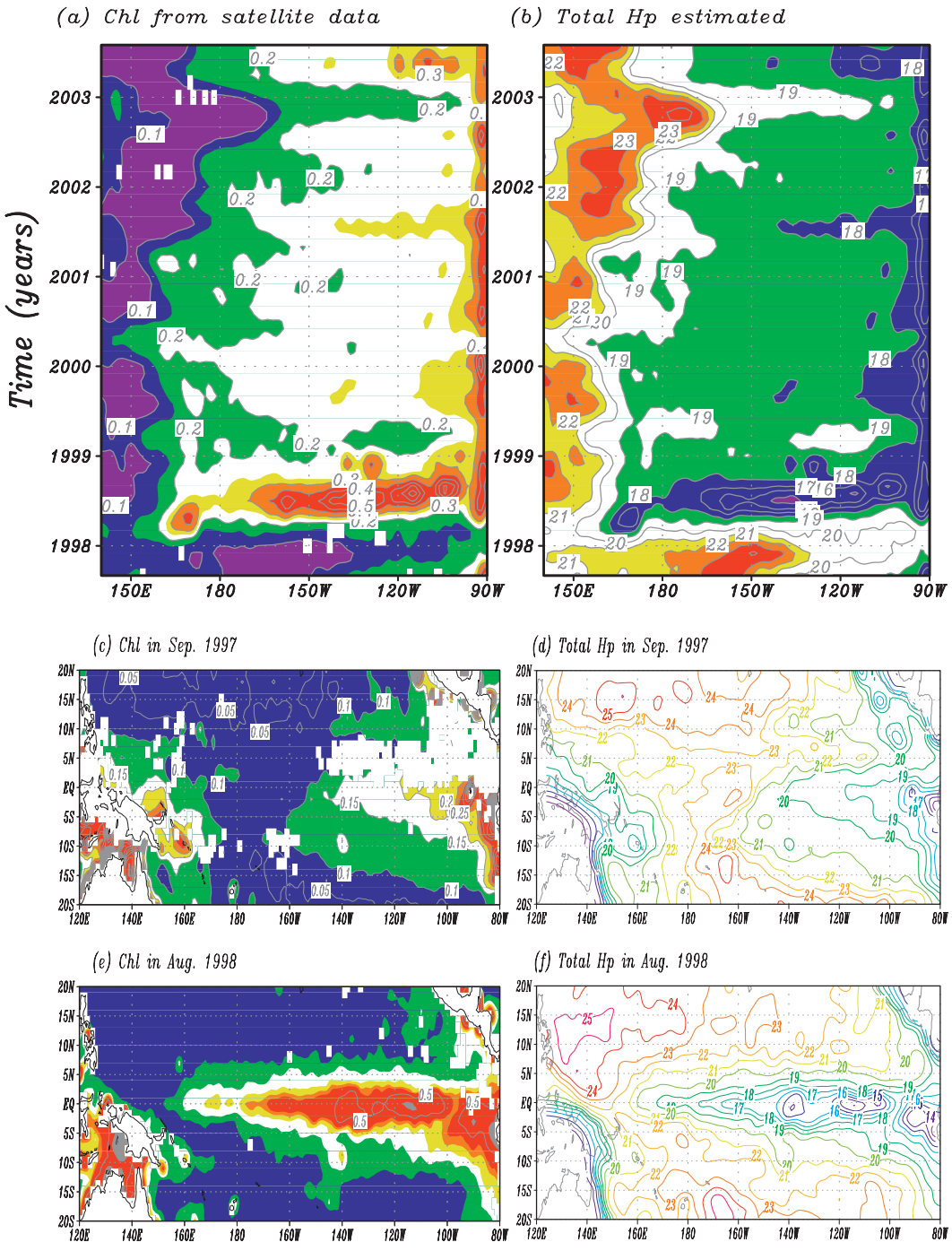

FIG. 1. The longitude–time plots along the equator during the period September 1997–August 2003 for (a) Chl concentrations and (b) the total H_p fields, and their corresponding horizontal distributions in September 1997 for (c) Chl and (d) H_p, and in August 1998 for (e) Chl and (f) H_p. The contour interval is 0.05 mg m^{-3} for Chl and 1 m for H_p.

Figure 2a illustrates the annual mean structure of derived H_p field in the tropical Pacific (also see Murtugudde et al. 2002; Ballabrera-Poy et al. 2007). Seasonal variations are shown in Ballabrera-Poy et al. (2007). The areas of small attenuation depth (<19 m) correspond to those of elevated biological activity in the coastal and equatorial upwelling regions. Values larger than 25 m are found in the oligotrophic subtropical gyres. The Beer–Lambert law implies that regions with the smallest attenuation depth correspond to the regions

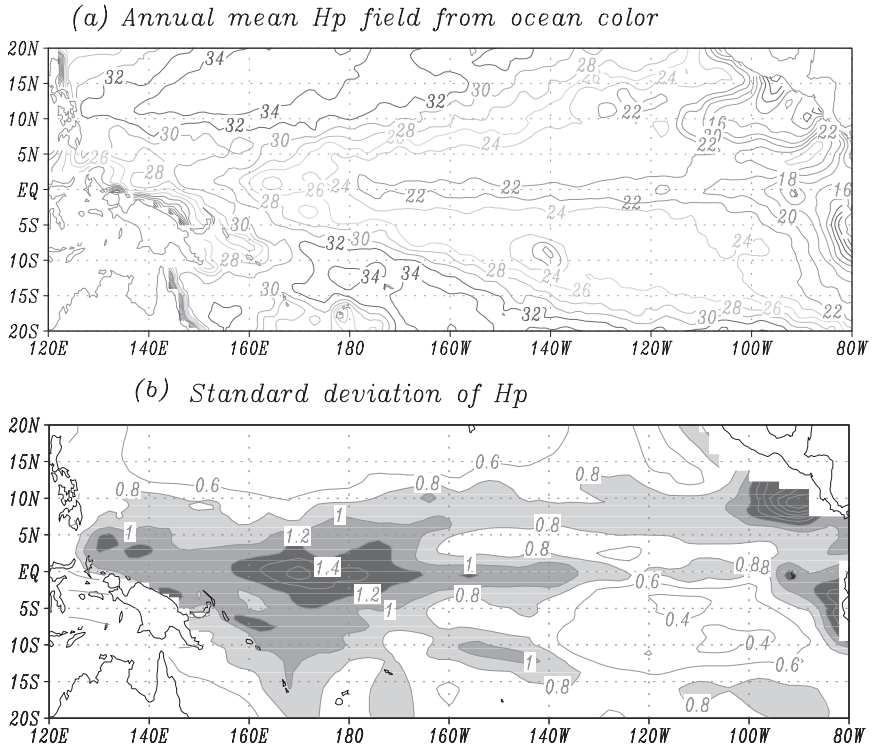

FIG. 2. The horizontal distributions of (a) the annual mean H_p field and (b) its standard deviation for interannual variability, estimated from the satellite ocean color data during the period September 1997–April 2007. The contour interval is (a) 2 and (b) 0.2 m.

where downwelling solar irradiance is absorbed the fastest.

Examples of interannual H_p anomalies are shown in Fig. 1 and Figs. 3–4 for temporal variations and snapshots in September 1997 and August 1988, which is representative of El Niño and La Niña conditions, respectively. Here, H_p exhibits a basinwide signal across the tropical Pacific basin, which is clearly dominated by El Niño and La Niña events. For example, during the 1997/98 El Niño, there was a reduction in upwelling and phytoplankton biomass; correspondingly, H_p increased dramatically over a very broad region in the equatorial Pacific, with a maximum enhancement of about 4 m in the central basin (Figs. 1d and 3a). When the physical conditions in the tropical Pacific shifted to La Niña in 1998, systematic changes took place in biological conditions. For example, during August 1998 when La Niña conditions prevailed in the tropical Pacific, the equatorial cold tongue developed strongly and extended westward, accompanied with significant increases in upwelling and phytoplankton biomass. The La Niña–induced H_p perturbations were negative in the equatorial Pacific (Figs. 1f and 4a).

The space–time evolution of interannual H_p variability along the equator can be more clearly seen in Fig. 5a. Large H_p perturbations are predominantly concentrated in the central and western regions. The spatial structure and temporal evolution exhibit a predominant standing pattern along the equator, indicating a local response of H_p to physical changes. In addition, it can be clearly seen that the range of interannual variations in H_p induced by ENSO exceeds that of seasonal variations (Ballabrera-Poy et al. 2007). A map of the standard deviation of interannual H_p variability is shown in Fig. 2b. The ocean biology–related interannual H_p variability is most pronounced over the central basin. The standard deviation of H_p in the Niño-4 and Niño-3 regions is 1.14 and 0.76 m, respectively.

Clear relationships exist between interannual variations in H_p and other physical fields (e.g., SST and SL). As demonstrated in Figs. 3–5, for their longitude–time sections along the equator and their horizontal patterns for El Niño and La Niña conditions, interannual variations in H_p and SST show a coherent covariability pattern during ENSO cycles, with the former following the latter closely. For example, as large-scale SST anomalies are generated in the tropical Pacific in association with ENSO, perturbations of H_p can be seen to be quick and almost simultaneous. During El Niño, SSTs are warm in the central and eastern equatorial Pacific, with a significant reduction

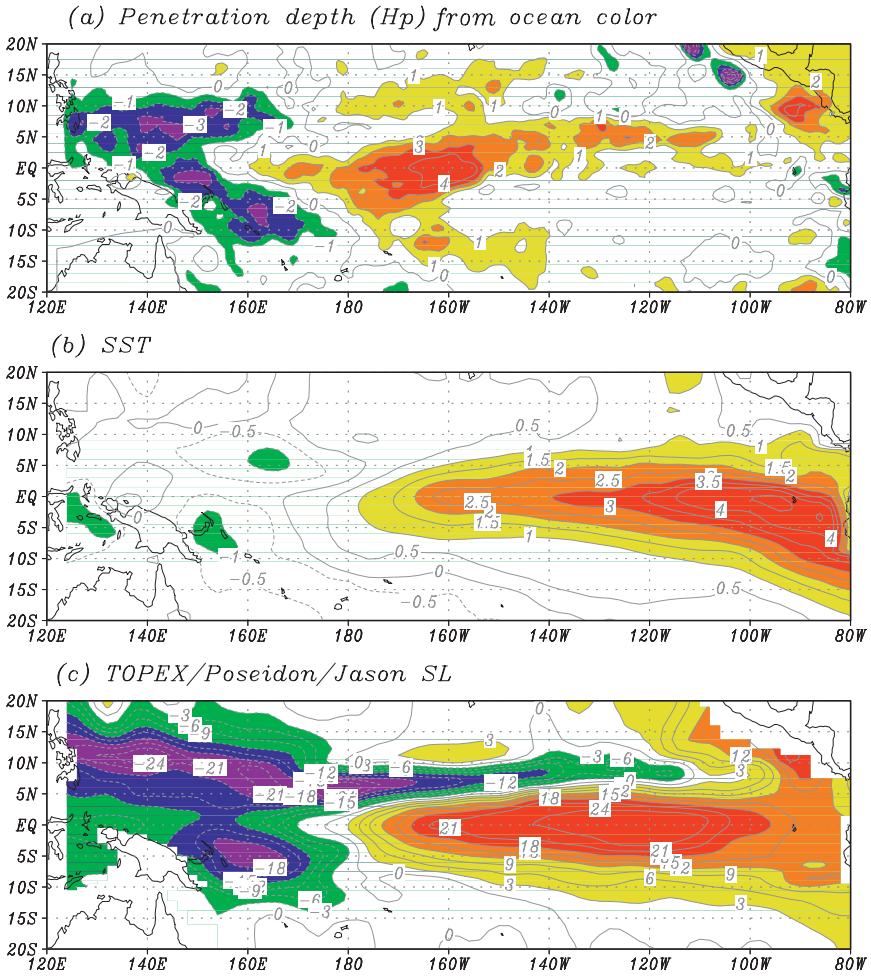

FIG. 3. The horizontal distributions for September 1997: (a) H_p, (b) SST, and (c) sea level anomalies in the tropical Pacific. The contour interval is (a) 1 m, (b) 0.5°C, and (c) 3 cm.

in upwelling and phytoplankton biomass. This is accompanied by a positive H_p anomaly in the central basin (Figs. 1d and 3a; an anomalously deep penetration of solar radiation). During La Niña when upwelling is strong and SSTs are cool with enhanced phytoplankton mass, the resultant H_p anomaly is negative in the central and eastern regions (Figs. 1f and 4a; an anomalously shallow penetration). As with SST (Fig. 5b), interannual variability in H_p exhibits a clear standing pattern (Fig. 5a) without significant zonal propagation in the tropical Pacific. Thus, interannual variations in H_p exhibit a positive correlation with SST.

The H_p also has a coherent relationship with SL, another important physical field for climate monitoring and modeling, which can be accurately depicted from TOPEX/Poseidon/*Jason-1* altimetry data (e.g., Nerem and Mitchum 2002). The spatial structure and temporal evolution of H_p and SL also indicate a coherent covarying pattern over the equatorial Pacific (Figs. 5a,c), which is expected because their interannual variations are both dominated by ENSO signals. However, there are occasions when variations in H_p and SL even exhibit out-of-phase behavior in the off-equatorial regions during ENSO evolution (Figs. 3–4). In addition, while H_p is dominated by a clear standing pattern (Fig. 5a), SL, in contrast, exhibits a pronounced phase propagation across the basin both on and off the equator (Fig. 5c). In addition, as represented by interannual variations in SST, SL, and H_p, clear differences are also evident in their spatial structure. For example, the maximum variability center of H_p is located in the central basin near the date line, while that of SST is located in the central and eastern equatorial region, and that of SL is located both in the east and west.

The space–time relationships among these fields suggest that interannual variations in H_p have a better correlation with SST than SL. This is further quantified by a simple correlation analysis (Fig. 6). On interannual time

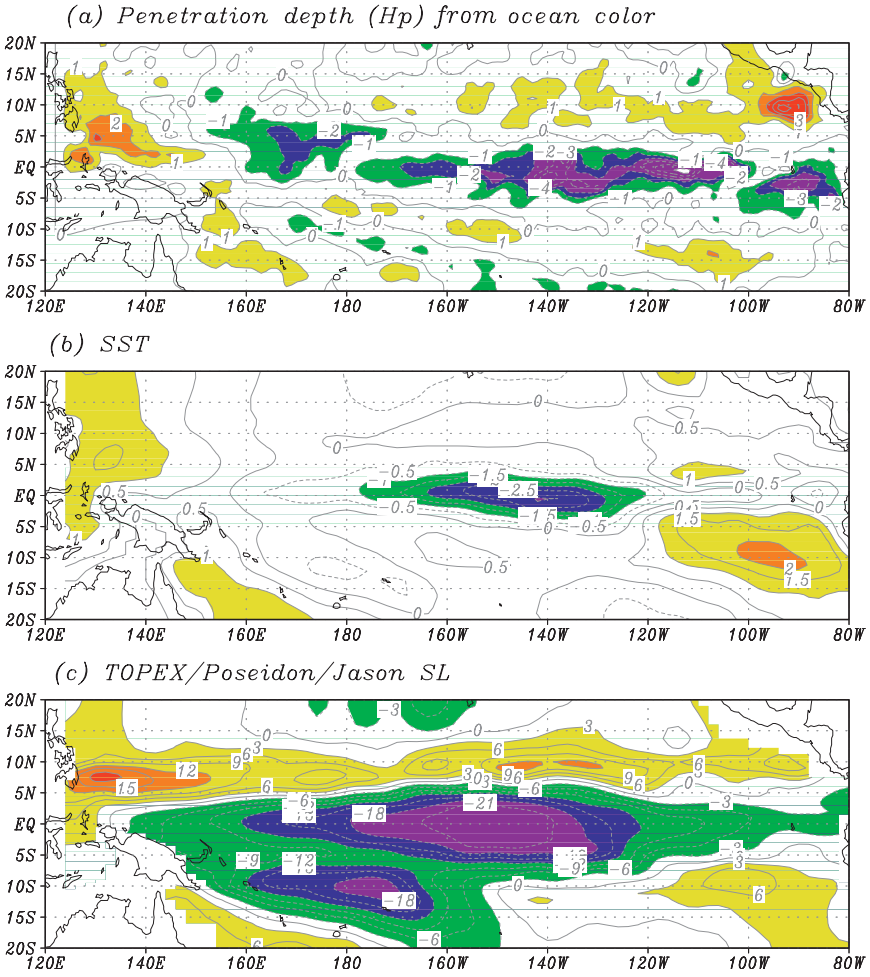

FIG. 4. As in Fig. 3, but for August 1998.

scales, both SST and SL fields exhibit high positive correlations with H_p in the equatorial Pacific. However, the extent to which H_p is positively correlated with SST and SL is evidently different. A much higher positive correlation is found between interannual variations in H_p and SST. For example, the anomaly correlation in the Niño-3 and Niño-4 region is 0.78 and 0.81 between H_p and SST, but is 0.62 and 0.63 between H_p and SL. Thus, SST can be a better physical parameter for representing H_p variability than SL.

3. Interannual covariability patterns between SST and H_p

The existence of coherent interannual covariability patterns between H_p and SST over the tropical Pacific can be further explored using more sophisticated statistical methods. To characterize their covarying relationships, an SVD analysis is applied to these two fields. This statistical approach has been used widely and successfully to extract coherent covariability patterns between coupled ocean–atmosphere fields (e.g., Syu et al. 1995; Chang et al. 2001; Zhang and Zebiak 2004; Zhang et al. 2005, 2006).

The SVD analysis technique adopted here is the same as that described in detail by Chang et al. (2001). In this work, the SVD analysis domain is confined over the tropical Pacific from 25°S to 25°N; its horizontal grid has a resolution of 1° in longitude and 0.5° in latitude. Over time, the SVD analysis is performed on all monthly SST and H_p data from September 1997 to April 2007. In more detail, interannual anomaly fields of SST and H_p are first normalized by their spatially averaged standard deviation to form a covariance matrix. The SVD analysis is then performed to get singular values and eigenvectors and their corresponding time coefficients. The first five SVD modes calculated from the covariance matrix of SST and H_p fields have singular values of about 1975, 371, 252, 134, and 117, with the squared covariance fraction of about 46%, 9%, 6%, 3%, and 3%, respectively.

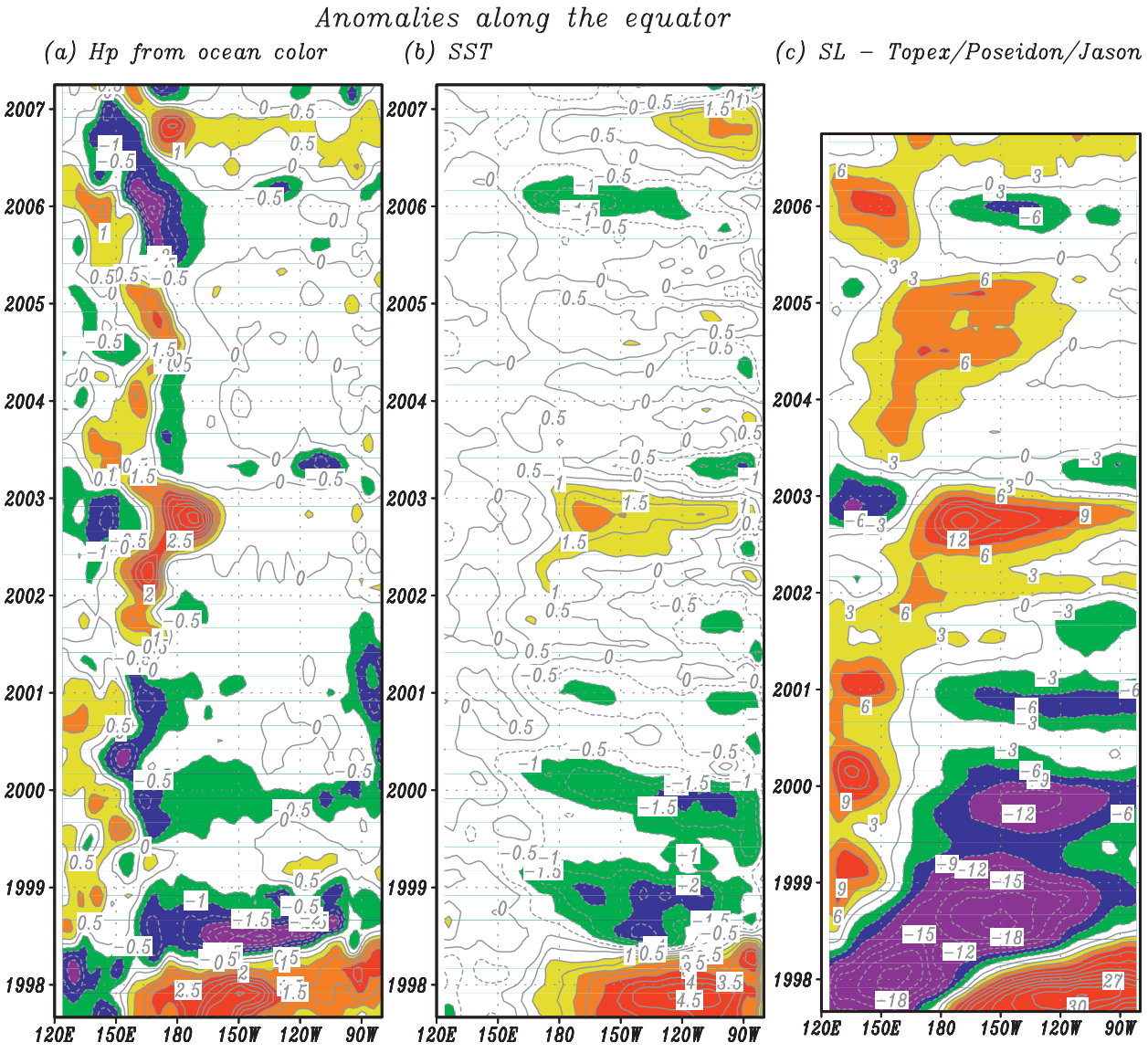

FIG. 5. Interannual anomalies along the equator: (a) H_p derived from the ocean color data, (b) SST, and (c) SL. Shown are data periods from September 1997 to April 2007 for H_p and SST, and from September 1997 to October 2006 for SL. The contour interval is (a) 0.5 m, (b) 0.5°C, and (c) 3 cm.

Figure 7 illustrates the singular values for the SVD modes 1–10, which represent the squared covariance accounted for by each pair of eigenvectors. The covariance (the singular values; Fig. 7a) decreases with SVD modes, which is not uniform. The sharp drop-off points can be seen after modes 2 and 4. The subsequent higher-order modes (beyond 5) have much smaller singular values, thus making fewer contributions to the covariance. The accumulated covariance (Fig. 7b) increases sharply for the first leading five modes but does so slowly for higher modes. The explained covariance by the first 2, 4, 5, and 10 modes are about 54%, 63%, 66%, and 74%, respectively.

Figure 8 exhibits the derived spatial eigenvectors of the first leading mode for SST and H_p, and their associated time series. The spatial structure and temporal evolution indicate that interannual changes in H_p and SST are clearly associated with El Niño and La Niña events in the equatorial Pacific. The spatial patterns (Figs. 8a,b) indicate that the primary mode of interannual H_p variability is composed of large H_p anomalies in the central Pacific (Fig. 8b), which covary with anomalous SSTs in the eastern and central equatorial Pacific (Fig. 8a). For example, a warm SST anomaly in the eastern equatorial Pacific (Fig. 3b) corresponds to a positive H_p anomaly in the central basin

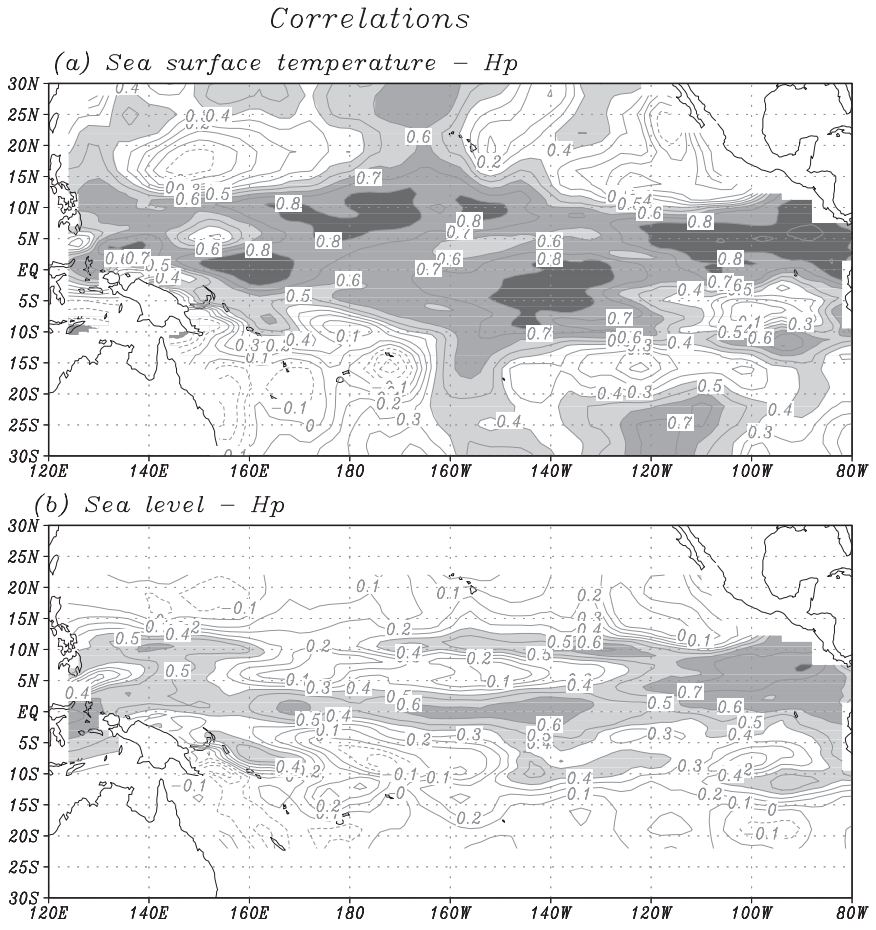

FIG. 6. Anomaly correlations (a) between H_p and SST, and (b) between H_p and SL. The calculation is made during the periods of September 1997–December 2006 for H_p and SST and September 1997–October 2006 for H_p and SL. The time series at each point have been smoothed by a 5-month running mean filter before calculating the correlations. The contour interval is 0.1.

(Fig. 3a). The temporal expansion coefficients (Fig. 8c) indicate that the first mode describes interannual variability associated with ENSO events. In particular, it is clearly evident that variations in H_p follow those in SST very closely (Fig. 8c). Calculated from the temporal expansion coefficients (Fig. 8c), the correlation coefficient is as high as 0.91. The second SVD mode (Fig. 9) also reveals a coherent relationship between SST and H_p, which is clearly ENSO related and represents a state with a different phase of ENSO evolution. Higher-order SVD modes (not shown) are typically smaller in amplitude, with less coherent structure in space and time.

4. A SVD-based empirical H_p model

The ENSO-dominated relationships between H_p and other physical fields in the tropical Pacific are explored to develop a simple statistical feedback model for the interannual variability of H_p. The purpose of such statistical modeling is to capture an interannual H_p response to a given change in the physical system. To do so, a physical field needs to be chosen that can represent and characterize interannual changes in the climate system well. SST serves this purpose.

As shown above, the SVD analyses indicate the existence of a coherent relationship between SST and H_p during ENSO evolution: in space, coherent patterns exist between H_p and SST across the tropical Pacific basin (Figs. 8a,b); in time, interannual variations in H_p follow those in SST closely (Fig. 8c). As often adopted, SST is a good indicator for changes in physical conditions in the tropical Pacific associated with ENSO. Also, SST variability generated in the ocean is the dominant forcing in terms of its coupling with the atmosphere. Moreover, as demonstrated above, H_p has higher correlation with SST than with SL. In this work, the demonstrated

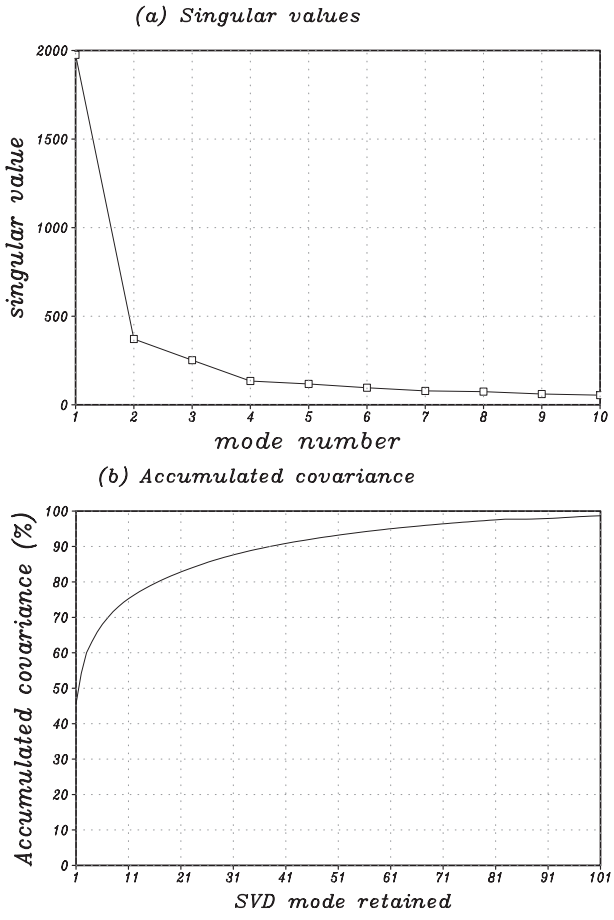

FIG. 7. The singular values of (a) modes 1–10 and (b) the accumulated covariance from the SVD analysis that is based on the covariance matrix calculated from time series of SST and H_p anomaly fields during the period September 1997–April 2007.

coherent relationships between SST and H_p are utilized to develop an empirical model for interannual H_p variability. This kind of statistical approach has been used widely and successfully in many large-scale tropical ocean–atmosphere modeling studies associated with El Niño (e.g., Barnett et al. 1993; Syu et al. 1995; Chang et al. 2001; Zhang and Zebiak 2004; Zhang et al. 2006).

As detailed by Syu et al. (1995) and Chang et al. (2001), the spatial eigenvectors and time series of the leading SVD modes derived from historical satellite data (Figs. 8–9) are used to construct a feedback model for H_p, which can be symbolically written as

$$H_p = \alpha_{H_p} \times F(\mathrm{SST})$$

where F represents an empirical relationship between interannual variations in H_p and SST, which are determined using the SVD analysis technique; and α_{Hp} is a scalar coefficient introduced to represent the strength of the H_p response to a SST anomaly. Accordingly, a given SST anomaly field can be converted to an H_p anomaly.

5. An evaluation of the empirical H_p model

The performance of the empirical H_p model can be sensitive to a variety of factors, including the retained modes and the periods that are taken for its training and for its application. A baseline model (H_p^{97-07}) is constructed for the period of 1997–2007, with the rescaling factor (α_{Hp}) set to be 1.0 and the first five leading SVD modes retained, which explain about 66% of the covariance (Fig. 7). An evaluation of this empirical model will be presented in this section.

a. Interannual H_p *variability*

Using the anomaly SST fields (Fig. 5b) as an input, an H_p response can be derived using the H_p^{97-07} model. Examples of the simulated H_p anomalies are illustrated in Figs. 10–11. It is evident that the model can capture the large-scale interannual H_p variability associated with ENSO very well. For example, the structure and phase of H_p variability simulated are well matched to those estimated from the original satellite data (Figs. 3–5). Apparently, however, the simulated H_p anomalies are somewhat weaker, smoothed, and less noisy, indicating that the selected SVD modes effectively act as a low-pass filter. Model performance is further evaluated in terms of anomaly correlation and root-mean-square (RMS) errors between H_p fields simulated from the empirical model and estimated from the observed Chl concentration data (Fig. 12). The empirical model has good simulation skill over the tropical Pacific; the correlation values exceeding 0.80 cover a broad region in the equatorial Pacific. Note that the skill is artificially high because the application periods are overlapping the training periods, and thus the skill (Fig. 12) should be considered as being representative of an upper limit of the empirical model simulation.

While the structure and phase of the H_p response are well captured, the simulated amplitude is evidently weak, about 60% of that estimated from the satellite data. Figure 12c shows the ratio of the standard deviation of interannual H_p variability simulated using the SVD model to that analyzed from satellite estimates (Fig. 2b). The amplitude of the simulated H_p anomalies is only about 60% of the original field (Fig. 2b); a significant fraction of covariance is thus lost in calculating interannual H_p variability using the empirical model from a given SST anomaly.

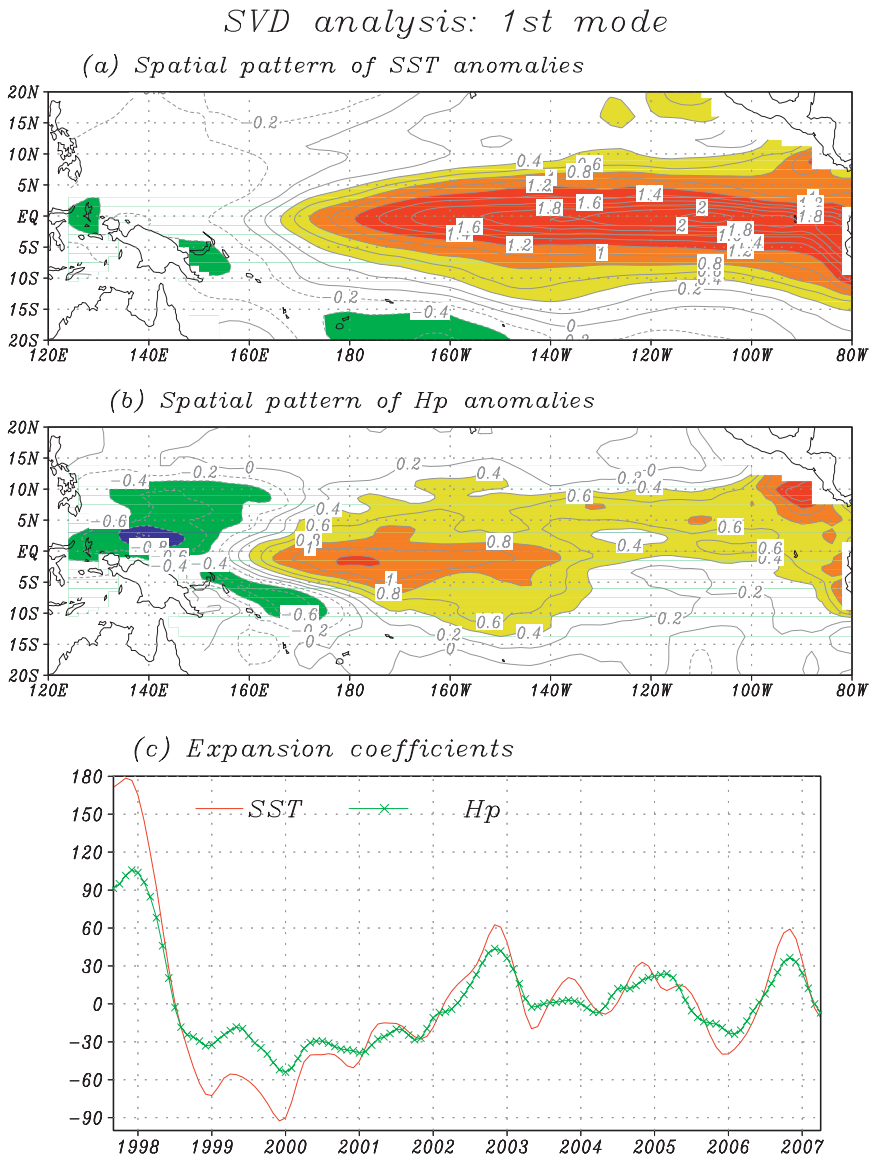

FIG. 8. The spatial patterns derived from the SVD analysis for the first pair of singular vector of (a) SST and (b) H_p fields, and (c) the time series associated with the first SVD mode. The SVD analysis is performed during the period September 1997–April 2007. The contour interval is 0.2.

b. *The effects of the SVD modes retained*

The historical databased statistical H_p model presented above is empirical in nature. As is inherent to any SVD-based method, its performance is sensitive to the numbers of SVD modes retained in the calculation. A major uncertainty in the H_p simulation is how many SVD modes should be retained, which can directly affect both the structure and amplitude of an H_p response to a given SST anomaly. To adequately capture the structure and amplitude, a sufficiently large number of SVD modes need to be retained; including too few SVD modes leaves important aspects of covariability unrepresented. However, retaining statistically insignificant SVD modes will contain non-ENSO-related noise that contaminates an H_p response signal. In this regard, fewer retained SVD modes are preferred in order to depict ENSO-related H_p signals. Therefore, a trade-off is needed in determining how many SVD modes should be retained.

A basic guidance in this practice is to see if, given an SST anomaly, an H_p response can be captured reasonably well in terms of the structure and amplitude as compared with the original satellite estimate. Also, the

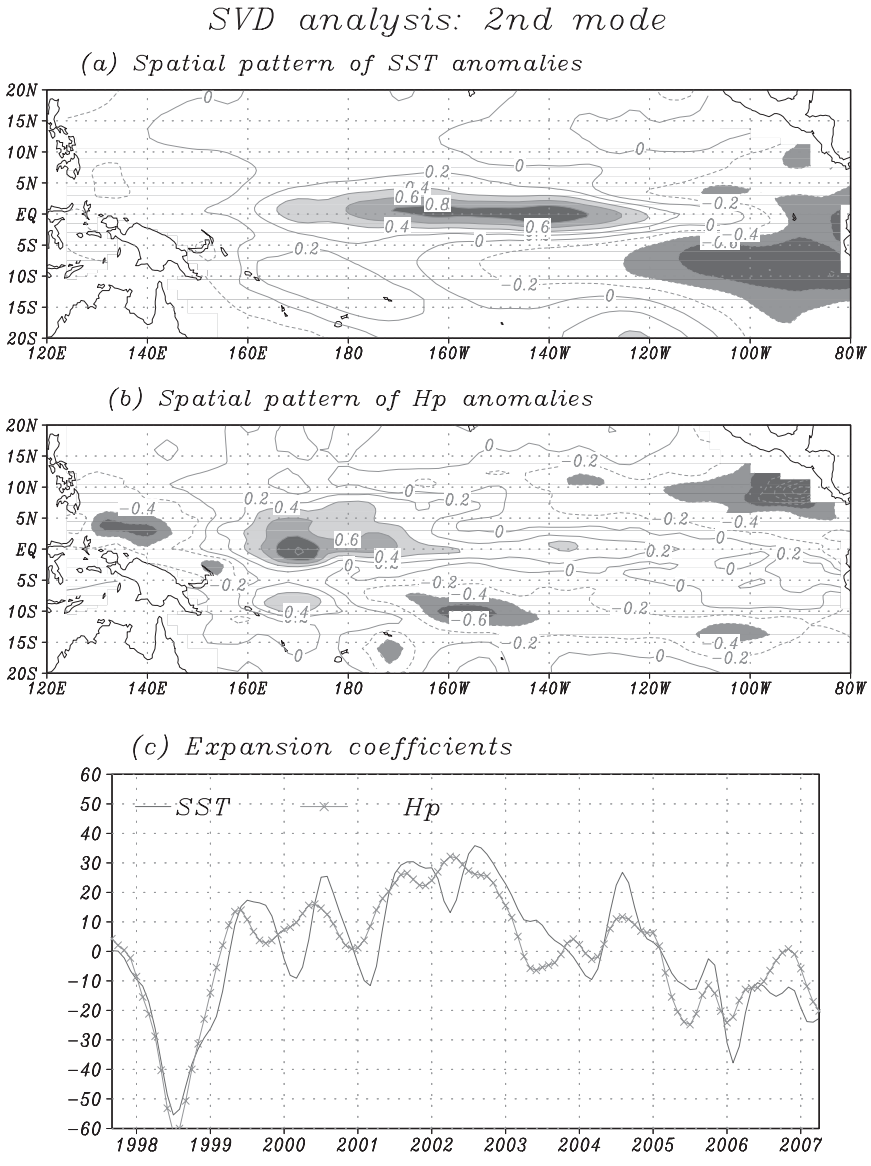

FIG. 9. As in Fig. 8, but for the second SVD mode.

subsequent singular values (Fig. 7a) and the spatial structure of eigenvectors (e.g., Fig. 8) can be guided to determine the number of SVD modes that are retained. As shown in Fig. 7, the decrease of the covariance (singular values) with the order of the SVD modes is not uniform; obvious drop-off points are seen after modes 2 and 4. Thus, a cutoff can be chosen at these modes for the empirical model to maximize the covariance to be represented. Furthermore, the examinations of the spatial eigenvectors indicate that the leading four modes all represent prominent signals both in SST and H_p over the equatorial Pacific. Thus, at least the first four SVD modes need to be retained for the SVD-based model to adequately capture anomalous H_p response to changes in SST.

We have examined the sensitivity of H_p simulations to the number of SVD modes retained. As an example, Fig. 10 displays the longitude–time sections of the simulated H_p fields along the equator, using the empirical H_p^{97-07} model with the first 2, 5, and 10 leading SVD modes retained; Fig. 13 illustrates their horizontal distributions for September 1997 estimated with the first 2, 10 and 20 SVD modes retained. It can be seen that the simulated structures are quite similar to each other in these calculations. For example, including only the first two modes can already represent the structure well (but the amplitude is apparently weak). The inclusion of the first five modes acts to improve the model simulation substantially (the first five modes account for about 66%

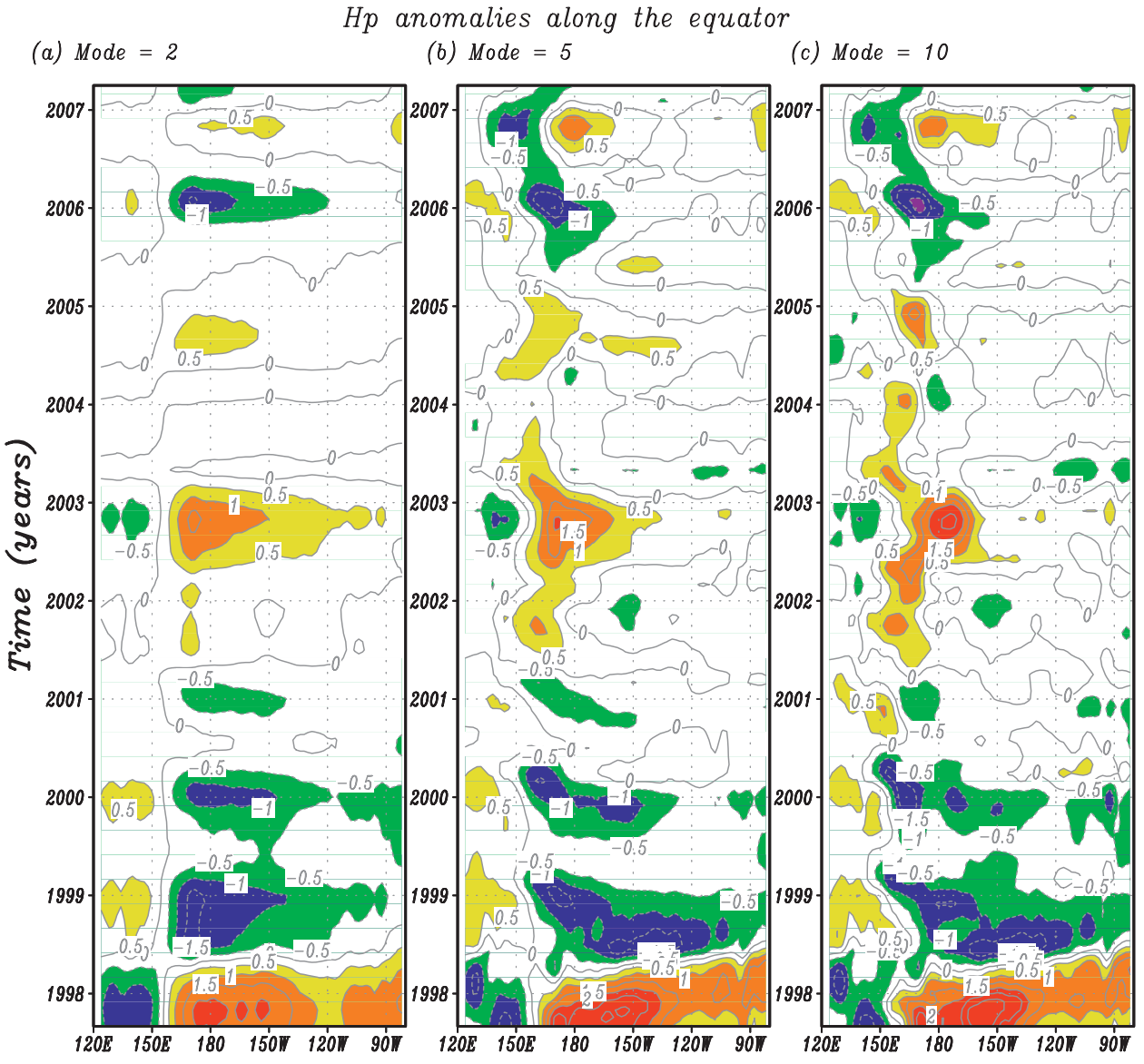

FIG. 10. The time–longitude sections of H_p anomalies along the equator, calculated using the empirical H_p^{97-07} model with the first (a) 2, (b) 5, and (c) 10 SVD modes retained. The contour is 0.5 m.

of the covariance). Further inclusion of the sixth and higher SVD modes does not significantly affect the structure and the amplitude (Figs. 10b,c). For example, the simulated H_p fields with the first 10 modes included (Fig. 13b) show no visual differences from those with the first 20 modes retained (Fig. 13c). Thus, retaining the first five SVD modes may be sufficient for the empirical H_p model to have adequate representations of interannual H_p variability in terms of the structure.

However, as compared with the original field (e.g., Figs. 3a and 5a), the simulated amplitude is systematically underestimated by a factor of about 2 (e.g., Figs. 10a and 11a). For example, the standard deviation of H_p in the Niño-4 and Niño-3 regions is only 0.63 and 0.38 m for the empirical model simulation with the first five SVD modes retained (the corresponding ocean color databased estimate is 1.14 and 0.76 m). As seen above, including more SVD modes is not an effective way to improve the amplitude simulation. The underestimation of the amplitude using the empirical model can be improved by utilizing the rescaling coefficient (α_{Hp}), which will be discussed below.

c. *The rescaling factor (α_{Hp})*

In this work, we take the SVD-based empirical approach to modeling H_p with SST fields chosen as

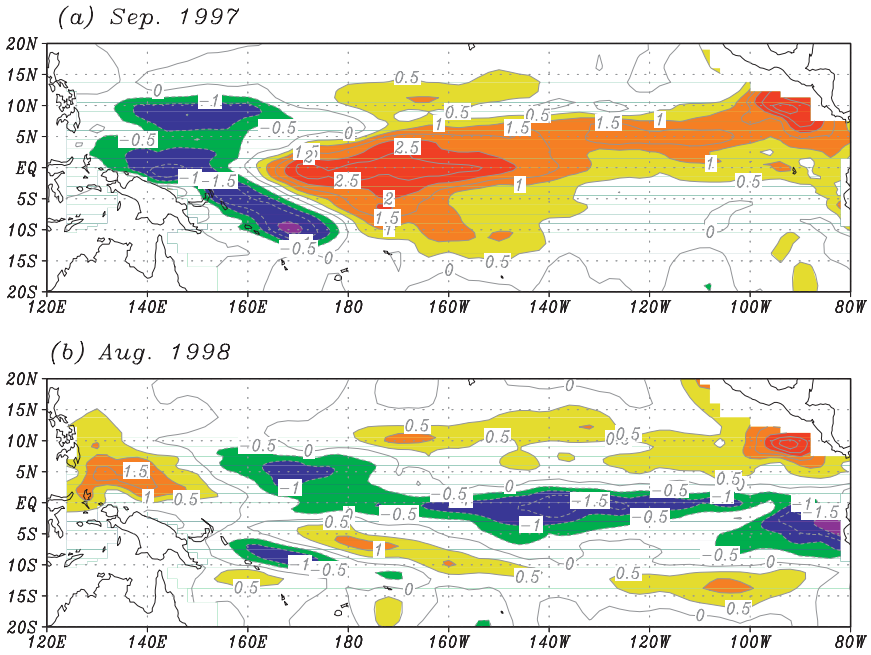

FIG. 11. The horizontal distributions of interannual H_p anomalies for (a) September 1997 and (b) August 1998, estimated using the empirical H_p^{97-07} model with the first five SVD modes retained. The contour interval is 0.5 m.

a predictor. This is based on the fact that there is a good relationship between interannual variations in H_p and SST over the equatorial Pacific in association with ENSO. However, SST may not be the only parameter affecting interannual H_p variability; the contributions of other important processes that are not captured by the SST–H_p relationships may be missing when using this empirical model to estimate interannual H_p anomalies, which can be responsible for model errors in the H_p simulations. As shown above, the amplitude of calculated H_p responses to a given SST anomaly is systematically weak as compared with that of the original satellite estimate. Sensitivity experiments indicate that including higher SVD modes is not an effective way to improve model simulation in terms of the amplitude. To resolve the underestimation issue of the amplitude, a scalar parameter α_{Hp} is introduced, which can be utilized to improve the model performance and enhance simulation skill. For example, the value of α_{Hp} is taken to be larger than 1.0 so that the response amplitude of H_p to a given SST anomaly can be increased (but the structure is not changed). This allows the amplitude to be rescaled back to match up with what is estimated from the satellite data. For instance, when taking $\alpha_{Hp} = 1.8$, the amplitude of simulated H_p variability can be well matched to that which is estimated. As a result, good simulations of interannual H_p anomalies can be achieved both in terms of the structure (which is determined by the first five leading modes) and of the amplitude (which can be flexibly adjusted by the rescaling factor). Note that this rescaling approach has been often utilized in the statistical modeling studies for large-scale wind simulations associated with ENSO (e.g., Barnett et al. 1993; Syu et al. 1995; Zhang et al. 2006).

d. Cross-validation studies

Note that by using the H_p model that is trained during the period of 1997–2007 to calculate the H_p fields for the periods that overlap the training periods, the skill for H_p simulations (e.g., as measured by an anomaly correlation) can be overly optimistic because historical information of H_p and SST variability covering the application period has already been included in the training period. We also perform other SVD analyses in which different periods are chosen to construct the empirical H_p models. For example, a corresponding H_p model is constructed for the period from January 1999 to April 2007 (denoted as H_p^{99-07}). Because the data for 1997 and 1998 are not included in the SVD analysis, the effects of the large 1997/98 ENSO events are excluded in the model construction. The first five SVD modes calculated from the covariance matrix of SST and H_p fields for this period have singular values of about 1341, 403, 264, 162, and 131, with the squared covariance fraction of about 42%, 13%, 8%, 5%, and 4%. The dominant modes of the corresponding

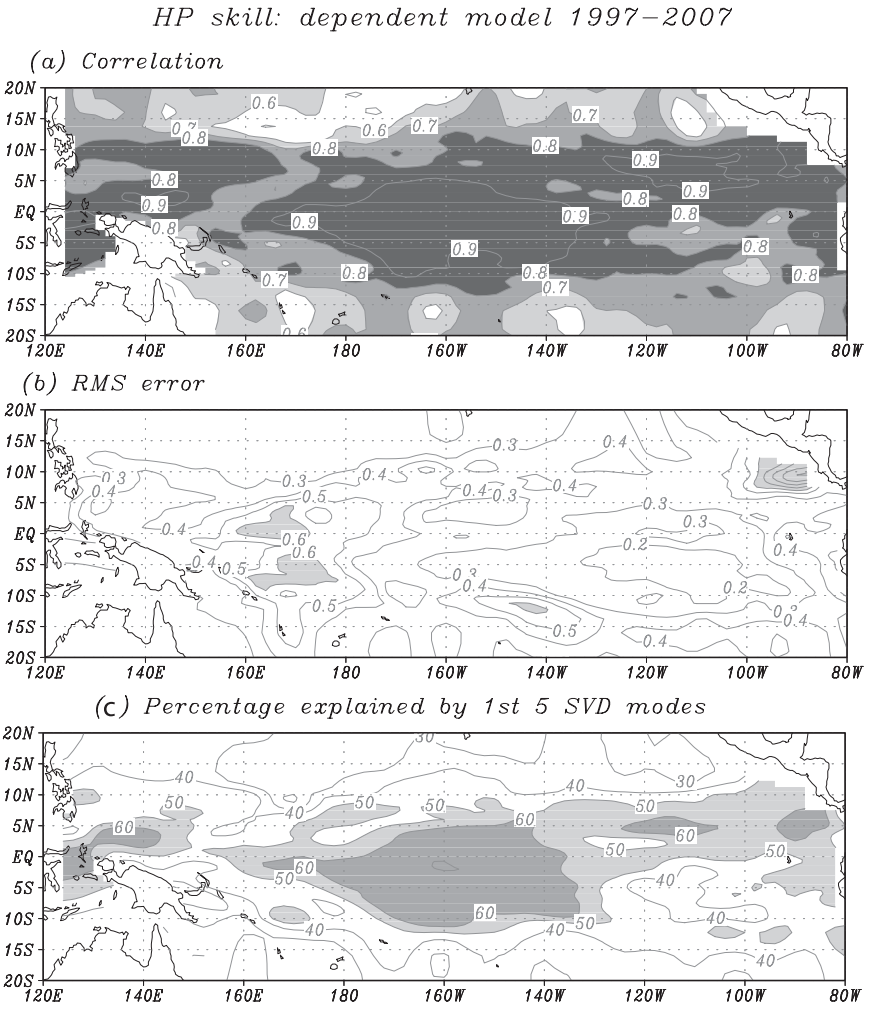

FIG. 12. (a) Anomaly correlation and (b) root-mean-square error between interannual H_p variability analyzed from the ocean color data and simulated using the SVD-based model with the first five modes retained, and (c) horizontal distribution of the variance percentage accounted for by the empirical model simulation, relative to that estimated from the ocean color data (Fig. 2b). The calculation is made during the period September 1997–April 2007. The time series at each point have been smoothed by a 5-month running mean filter before the calculations. The contour interval is (a),(b) 0.1 and (c) 10%.

spatial eigenvectors of the first leading mode derived for SST and H_p, and their associated time series, are clearly ENSO related (not shown), with their coherent covarying patterns similar to those in Fig. 8. Also, the H_p anomaly patterns of the 1997/98 event using the H_p^{99-07} model can be captured reasonably well, compared with those observed from satellite data (Figs. 3–4). This suggests that the performance of the empirical H_p model is neither duly sensitive to the training period selected, nor to the application period. Although the periods selected for the cross validation are too short to produce stable statistics for the simulation skill, the empirical H_p model appears to be quite successful in calculating interannual H_p anomalies in response to ENSO-induced SST anomalies.

6. Representing ocean biology–induced heating effects using the empirical model: An example

Ocean and coupled ocean–atmosphere model simulations in the equatorial Pacific are known to be sensitive to variations in the vertical solar heat flux divergence in the upper ocean. The large range of interannual H_p variability induced by El Niño and La Niña events is expected to modulate the vertical penetration of solar radiation in the upper ocean. In this section, as an example, we illustrate how the derived empirical H_p model can be utilized to represent the ocean biology–induced heating effect through a diagnostic analysis based on a hybrid coupled model (HCM) simulation of the tropical Pacific; the HCM

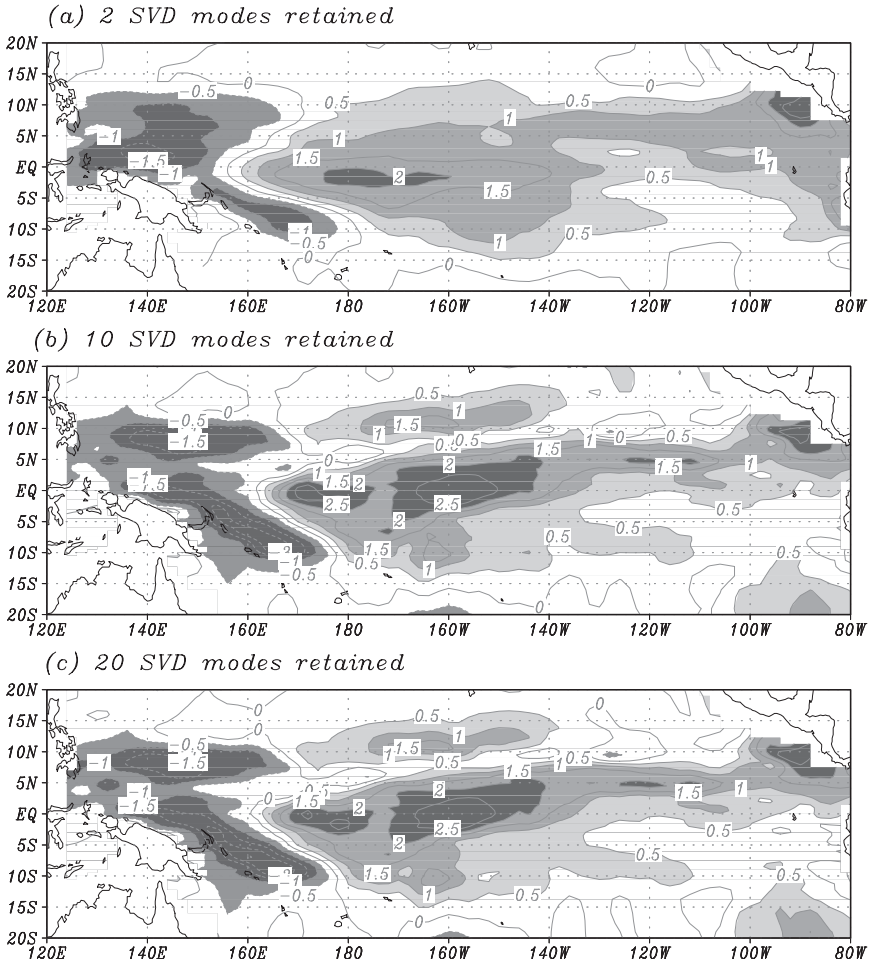

FIG. 13. The horizontal distributions of interannual H_p anomalies for September 1997 estimated using the empirical H_p^{97-07} model with the first (a) 2, (b) 10, and (c) 20 SVD modes retained. The contour interval is 0.5 m.

consists of the Gent–Cane ocean general circulation model (OGCM) and an SVD-based empirical model for wind stress anomalies (Zhang et al. 2006). As described in Zhang and Busalacchi (2009), the HCM can well simulate interannual variations associated with ENSO. Figure 14a illustrates examples of the simulated interannual SST anomalies along the equator, which exhibit warming and cooling with about 4-yr oscillation periods.

Using the anomaly SST field (Fig. 14a) as an input, interannual H_p anomalies can be estimated accordingly using the empirical H_p^{97-07} model with the first five SVD modes retained and $\alpha_{Hp} = 1$. Figure 14b shows the longitude–time section of interannual H_p anomalies along the equator. Large H_p anomalies are seen across the tropical Pacific basin in association with ENSO, with coherent space–time relationships with SST. For example, during El Niño, a positive H_p anomaly is seen in the central and eastern equatorial Pacific, which is accompanied with a negative H_p anomaly in the far western region. During La Niña, an opposite anomaly pattern is evident for H_p. The structure and evolution of interannual H_p variability are in good agreement with those seen in the satellite-based estimates (e.g., Fig. 5), but the amplitude is apparently smaller when $\alpha_{Hp} = 1$ is taken. The calculated H_p field can then be utilized to diagnose its direct effect on ocean biology–related heating in the upper ocean.

In the formulation of the OGCM (e.g., Chen et al. 1994), several ocean biology–related heating terms in the upper ocean are explicitly associated with H_p, including the penetrative solar radiation flux out of the bottom of the mixed layer (Q_{pen}), which can be written as

$$Q_{\text{pen}}(H_m, H_p) = Q_{\text{sr}}[\gamma \exp(-H_m/H_p)],$$

where Q_{sr} is the incoming solar radiation flux at the sea surface, H_m is the mixed layer depth, H_p is the

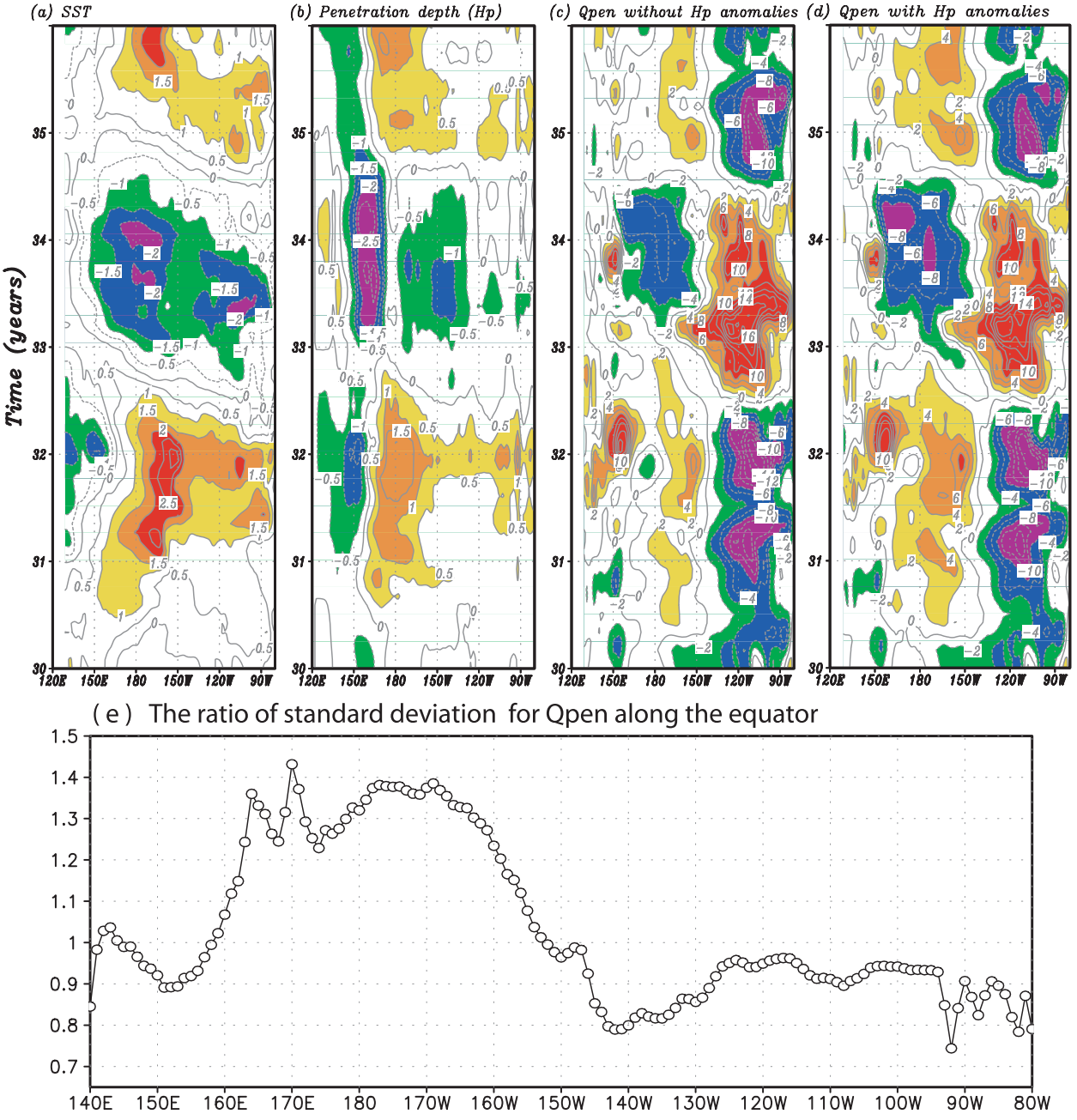

FIG. 14. Interannual anomalies along the equator from an HCM simulation: (a) SST, (b) H_p, and Q_{pen} calculated (c) without and (d) with the effect of the interannual H_p anomalies taken into account. The H_p field is estimated using the empirical H_p model with the first five SVD modes retained and $\alpha_{Hp} = 1.0$. (e) The zonal distribution of the ratio of the standard deviation along the equator for interannual Q_{pen} variability calculated from a 26-yr HCM simulation with and without the effect of interannual H_p variability [$Q_{\text{pen}}(H_m, H_p)$ and $Q_{\text{pen}}(H_m, \overline{H}_p)$]. The contour interval is (a) 0.5°C, (b) 0.5 m, and (c),(d) 2 W m^{-2}.

penetration depth, and γ is a constant (=0.33) denoting the fraction of the solar radiation available to penetrate to depths beyond the very first centimeters of the sea surface. As indicated, Q_{pen} is a function of both H_p and H_m fields, which exhibit well-defined space–time structure across the tropical Pacific [e.g., see examples for H_p field in Fig. 14b and for H_m field in Zhang and Busalacchi (2009), respectively]. As expressed above, the structure and variation of H_m and H_p exert a direct influence on Q_{pen}. For example, when H_m decreases (increases), there is a corresponding increase (decrease) in the solar radiation flux out of the bottom of the mixed

layer. In contrast, the effect of H_p on Q_{pen} is opposite to that of H_m, that is, the decrease (increase) in H_p acts to reduce (increase) the value of Q_{pen}.

The empirical H_p model is utilized to explicitly calculate interannual H_p variability, which, in conjunction with H_m, can then be used to illustrate their combined effects on interannual Q_{pen} variability. To do so, we first calculate the Q_{pen} field with H_p taken as its annual mean ($\overline{H_p}$, Fig. 2a), denoted as $Q_{\text{pen}}(H_m, \overline{H}_p)$. Figure 14c presents the interannual Q_{pen} anomalies along the equator calculated with the effect of interannual H_p variability explicitly excluded. As seen, Q_{pen} undergoes interannual fluctuations during ENSO cycles, which are determined by those of H_m. For example, as with interannual variations in H_m (Zhang and Busalacchi 2009), those in Q_{pen} also show a similar see-saw pattern zonally along the equator, with a zero crossing line around 150°W. In the central equatorial Pacific, a negative Q_{pen} anomaly is seen during La Niña when the mixed layer is anomalously deep (a low Q_{pen} value indicates less penetration of solar radiation out of the base of the mixed layer); a positive Q_{pen} anomaly emerges during El Niño when the mixed layer (ML) is anomalously shallow (a high Q_{pen} value indicates more penetration throughout the base of the mixed layer, and thus more heating directly to the subsurface layers). An opposite anomaly pattern is seen in the eastern equatorial region (east of 150°W), where interannual Q_{pen} variability is characterized by a negative anomaly during El Niño and a positive anomaly during La Niña. As expected, interannual variations in Q_{pen} are negatively correlated with those in H_m during ENSO evolution.

To see the direct effect of H_p on Q_{pen}, we then perform another calculation for Q_{pen} in which interannual H_p variability estimated from the SVD-based empirical model is explicitly taken into account, denoted as $Q_{\text{pen}}(H_m, H_p)$, where $H_p = \overline{H_p} + H_p'$. Figure 14d presents the calculated interannual Q_{pen} anomalies along the equator. Although the interannual variability of Q_{pen} is dominated by that of H_m, a clear effect of H_p on Q_{pen} can be seen during ENSO cycles, as compared with the case in which interannual H_p variability is not included (Fig. 14c).

In the central basin where the amplitude of interannual H_p variability can be about 10%–20% as large as that of H_m, H_p is expected to exert a significant influence on Q_{pen}. Because interannual variations in H_m and H_p tend to be out of phase in this region, their effects on Q_{pen} are in phase. During El Niño, a positive H_p anomaly, seen in the central basin, acts to enhance the positive Q_{pen} anomaly associated with a negative H_m anomaly. During La Niña, an opposite pattern can be seen among these anomaly fields. As a result, interannal H_p anomalies tend to enhance Q_{pen} variability in the central Pacific during ENSO cycles, making it more positive during El Niño and more negative during La Niña, and thus leading to a larger interannual Q_{pen} variability. As shown in Fig. 14e, interannual Q_{pen} variability can be significantly enhanced by the effect of interannual H_p variability (more than 20% in the central equatorial region between 160°E and 160°W). Quantitatively, the standard deviation of interannual H_p variability from 160°E to 160°W on the equator (averaged between 0.5°N and 0.5°S) is 1.39 m for the satellite databased estimate and is 0.89 m for the empirical H_p model simulation with the first five SVD modes retained and $\alpha_{Hp} = 1$. Correspondingly, the standard deviation of interannual Q_{pen} variability averaged in the same region is 3.7 W m^{-2} for the $Q_{\text{pen}}(H_m, \overline{H}_p)$ case (the interannual H_p effects are not included), and 4.2 W m^{-2} for the $Q_{\text{pen}}(H_m, H_p)$ case (the effects are explicitly taken into account). If $\alpha_{Hp} = 2$ is taken so that the amplitude of interannual H_p variability from the empirical model can match up with that estimated from satellite data, then the corresponding standard deviation of Q_{pen} is 4.8 W m^{-2} in the central basin. Compared with the $Q_{\text{pen}}(H_m, \overline{H}_p)$ case, the standard deviation of interannual Q_{pen} variability in the central equatorial Pacific increases by 14% with $\alpha_{Hp} = 1$ and 30% with $\alpha_{Hp} = 2$. Thus, a penetration depth estimated by using the empirical H_p model can be seen to yield a significant difference in the heating terms in the central equatorial Pacific, as illustrated for the Q_{pen} field here.

In the eastern basin (east of 150°W), interannual variations in H_m and H_p tend to be in phase and their effects on Q_{pen} are thus opposite. Because the amplitude of interannual variations in H_p is smaller relative to that in H_m, interannual Q_{pen} variability is dominated by the H_m effect there, with a small offset by H_p. During La Niña when the ML is shallow, Q_{pen} exhibits a positive anomaly (see Fig. 14c; an indication of more penetration of solar radiation into the subsurface layers); the effect of a negative H_p anomaly acts to reduce the positive Q_{pen} anomaly (Fig. 14d). During El Niño, when the ML is deep, Q_{pen} tends to be negative (see Fig. 14c; an indication of less penetration out of the mixed layer and less direct heating to the subsurface layers); the effect of a positive H_p anomaly leads to a reduced negative Q_{pen} anomaly (thus being less negative). As a result, interannual Q_{pen} variability is reduced by the H_p effect in the eastern equatorial Pacific (generally less than 10%, as shown in Fig. 14e).

7. Discussion and conclusions

Ocean biology–induced heating effects and bioclimate coupling in the tropical Pacific have been of much recent

interest because of their potential for the modulation of ENSO. Physically, its effects on heating in the upper ocean can be represented by the penetration depth of solar radiation (H_p). While interannual variability in the physical system (e.g., SST) is well understood, simulated, and even predictable about 6 months or more in advance (e.g., Zhang et al. 2005), studies on biological processes and their feedback effects on physics in the ocean are still in the early stage. At present, ocean models have considerable difficulty in accurately representing biogeochemical variability. For example, current comprehensive ocean biogeochemistry models still cannot realistically depict interannual H_p anomalies during ENSO cycles. As a result, most global climate models have not adequately taken into account the effects of interannual H_p variability. In particular, the effects have not been included in all of the coupled models currently used for real-time ENSO predictions. The advent of space-based satellite observations has provided an unprecedented basinwide data of not only physical fields, but also biological parameters in the ocean. Now, interannual H_p variability can be routinely derived from remotely sensed Chl data. Previously, derived spatially and seasonally varying H_p fields have been utilized in ocean and coupled ocean–atmosphere model simulations; the large effects are found on ocean and climate simulations in the tropical Pacific, with strikingly model-dependent and even conflicting results.

In this work, we focus on interannual H_p variability in the tropical Pacific. Satellite observations during the period of September 1997–April 2007 are used to characterize interannual H_p variability and to quantify its relationships with changes in physical parameters, including SST and SL. As expected, interannual H_p variability is dominated by ENSO signals, with its largest variability region located in the central equatorial Pacific. The pattern and structure show a coherent relationship with physical fields in the tropical Pacific, with better correlation with SST than SL. Then, an SVD analysis technique is adopted to extract dominant interannual covariability patterns between SST and H_p. The close relationships between SST and H_p fields are further utilized to construct an empirical anomaly model for H_p at interannual time scales. Then, a given SST anomaly field can be converted to an H_p response. It is demonstrated that the empirical H_p model can capture interannual H_p variability well, as directly estimated from satellite measurements, including the well-defined spatial structure and time evolution. However, the simulated amplitude is underestimated significantly. Some sensitivity and validation experiments are performed to demonstrate the robustness and usefulness of the empirical H_p model.

The empirical H_p model we propose here is simple and computationally economical. The adopted SVD analysis technique allows for a nonlocal, SST-dependent, and spatially and temporarily varying representations of H_p field at interannual time scales. Together with the climatological H_p field that can be estimated from multiyear ocean color data, its total field (composed of its climatological part and interannual anomaly part) can be prognostically determined, allowing for the parameterization of the effect of Chl containing biomass on the penetrative solar radiation, and, further, on ocean thermodynamics and dynamics in the upper ocean of the tropical Pacific. In addition, it is clearly demonstrated that the Chl concentration data from SeaWiFS can have dynamical implications for ocean biophysical coupling in the tropical Pacific. Also, it is evident that resolving ocean biophysical coupling issue needs to involve both physical and biological fields, indicating a clear need for a broad range of observations and scientific interactions among different scientific communities.

Several concerns arise in the statistical modeling for H_p using the SVD-based empirical model from a given SST anomaly. This statistical modeling approach can be justified because there is a good relationship between interannual variations in H_p and SST over the equatorial Pacific on interannual time scales associated with ENSO. Being better correlated with H_p than SL, SST is chosen as the representative of physical changes in the climate system from which an empirical feedback model for H_p is derived. However, SST may not be the only parameter affecting interannual H_p variability; other physical and biological processes, independent from SST effects, can also be important, which may have not been adequately represented in the SST–H_p relationships. A calculation of H_p in terms of SST anomaly only using an empirical model derived from historical data implies that any processes contributing to H_p variability will be empirically included in the SST–H_p relationship, in so far as these processes are reflected in interannual SST variability. This may lead to a biased estimation for H_p. The modeling results indicate that these possible aliasing problems are not serious when using the empirical H_p model to calculate H_p from a given SST anomaly. As has been shown above, the empirical H_p model performs well in capturing interannual anomalies associated with ENSO, which are in good agreement with satellite-based data.

Another concern is with the SVD mode cut-off error using the empirical model to calculate interannual H_p anomalies. As shown above, the structure and amplitude of simulated interannual H_p variability can be sensitive to several factors, including the SVD modes that are retained. Modeling experiments indicate that the spatial

structure of interannual H_p variability is well captured by the first few leading modes, but the amplitude is not (the amplitude simulated is still underestimated significantly when a large number of SVD modes are retained). This suggests that the contributions of other important processes that have not been taken into account by the SVD-based SST–H_p relationships may be missing when using this empirical model, leading to a systematic underestimation of simulated H_p variability. Sensitivity experiments indicate that including higher SVD modes is not an effective way to improve model simulation in terms of the amplitude; doing so can actually introduce noises that are not relevant to ENSO signals. To resolve the underestimation issue of the amplitude, the introduced rescaling coefficient α_{Hp} can be utilized to adjust the H_p amplitude in order to partially compensate for the loss of the covariance in the SVD-based model calculation. For example, the value of α_{Hp} can be taken to be larger than 1.0 so that the response amplitude of H_p to a given SST anomaly is increased, allowing for the empirical model simulation to match up with what is estimated from the satellite ocean color data. As such, good simulations of interannual H_p variability in response to a given SST anomaly can be achieved both in terms of the structure (which is determined by the first few leading SVD modes) and the amplitude (which can be adjusted by the rescaling factor), respectively. Note that the specifications of these statistical model parameters (the SVD modes retained and the rescaling factors, α_{Hp}) can be rather arbitrary and are certainly not an optimized one; a better optimization procedure for these parameters may be necessary to improve model performance more effectively.

Also, the performance of the empirical H_p model constructed from historical data can be compromised by sampling errors, which come from a variety of sources, including short time records in which there are only a small number of independent realizations of interannual events associated with ENSO. For example, sampling errors in time are known to cause uncertainties in the eigenvalues of the cross-covariance matrix in empirical orthogonal functions (EOFs; North et al. 1982); these results can apparently apply to SVD analyses presented here (in our case, the singular values). Indeed, the period used in our SVD analysis (1997–2007) is too short to adequately sample multiple ENSO cycles, and thus may not accurately represent covariability patterns between SST and H_p as extracted using the SVD analysis. Also, the short data record limits the number of SVD modes to be retained in the H_p modeling. A longer record should, in theory, lead to a more accurate representation of SVD modes and thus allow retention of more higher-order SVD modes, helping to resolve the underestimation problem for the empirical H_p model.

Further improvements and applications of the empirical H_p model are underway. For example, in this paper we present a purely statistical modeling study on the interannual variability of H_p, with a lack of process understanding. Nevertheless, based on the relationships among the interannual variations in SST, SL, and H_p that have been analyzed, some limited physical insight into the processes is of value to further process studies. For example, analyses indicate that interannual variations in SST, SL, and H_p have clear differences in their spatial structures, suggesting that different dominant processes are at work. As is well understood (e.g., Zebiak and Cane 1987), interannual variations in SST are dominantly determined by mixing and upwelling in the equatorial Pacific, while those in SL are determined by thermocline variability. The fact that interannual variations in H_p are better correlated with SST than SL indicates that the processes important to SST, including the mixing and upwelling, also play a dominant role in interannual H_p variability. Because H_p is less correlated with SL than SST, the thermocline variability can be a less important factor affecting interannual H_p variability. A dynamical biogeochemical model for H_p is clearly needed in order to investigate the detailed processes that are responsible for interannual H_p variability in the tropical Pacific.

Also, in this paper, we focus on illustrating the feasibility of using historical satellite ocean color data to parameterize ocean biology–induced heating effects in the upper ocean. Here H_p is chosen because it is a primary parameter in coupling biology to physics via the attenuation of solar radiation in the upper ocean. Mathematically, this parameter is involved with some formulation of the attenuation depth of solar radiation (e.g., exponent H_p); physically, this field is affected by Chl containing biomass in the upper ocean, but its relationship with the penetrative effects of solar radiation is presumably empirical in nature and difficult to represent/interpret precisely. To quantify the ocean biology–induced heating effects, we adopt a very simple algorithm that yields H_p from remotely sensed Chl data: a single absorption coefficient is taken to account for the average attenuation over the visible band (380–700 nm). As already examined by previous studies (e.g., Stramska and Stramski 2005), the relationships between H_p and Chl are very complicated, involving variable absorption coefficients for different frequency bands. A sophisticated algorithm is clearly needed to represent the relationship between H_p and Chl more accurately.

Also, a similar statistical modeling approach can be directly applied to other more biologically visible fields in a straightforward way. For example, Chl concentration is a parameter that is a primary component of

biogeochemical/ecosystem models; it can be chosen for a statistical modeling target as well so that a corresponding empirical model between SST and Chl can be constructed to capture variations in ocean biology. Then, a more general SST–Chl model can be utilized by a number of solar penetration parameterizations to represent the effects on physics more accurately (e.g., Stramska and Stramski 2005). Nevertheless, because H_p can be determined from the Chl data, the results inferred with the H_p analysis and modeling from this work can be equivalently applied to the Chl field, including the dominance of interannual variability by ENSO signals, the largest variability center located in the central equatorial Pacific, and a coherent covariability pattern with SST as revealed by SVD analyses.

Furthermore, large interannual H_p variability is seen in the tropical Pacific, a region that is important to large-scale coupled climate variability associated with ENSO. As have been demonstrated by previous studies (e.g., Lewis et al. 1990), the ocean heating effects induced by large perturbations in phytoplankton biomass make a significant contribution to the heat balance in the equatorial Pacific. Thus, it is necessary to adequately take into account the ocean biology–induced climate feedback in coupled ocean–atmosphere models. The empirical H_p model we derive here can be utilized to parameterize the ocean biology–induced heating effects. For example, it can be used to serve as a simple ocean biological component for bioclimate coupling in a coupled ocean–atmosphere model, in which interannual H_p variability can be generated internally and interactively in response to a change in physics (i.e., SSTs). In addition, ENSO has been observed to change significantly from one event to another; many physical factors in the climate system have been identified that can contribute to the modulation of ENSO (e.g., Zhang et al. 1998, 2008; Zhang and Busalacchi 2008, 2009). As a biological factor, ocean biology can play a role in modulating ENSO, as have been recently demonstrated by previous modeling studies (e.g., Timmermann and Jin 2002; Zhang et al. 2009). Further modeling studies are clearly needed to better describe and understand the modulating impacts of ocean biology–induced feedback and bioclimate coupling on interannual variability and predictability in the tropical Pacific.

Acknowledgments. We appreciate the input from Tony Busalacchi and J. Ballabrera-Poy. We appreciate the assistance for TOPEX/Poseidon/*Jason-1* sea level data from E. Hackert and G. Michum. The authors wish to thank the two anonymous reviewers for their numerous comments that helped improve the original manuscript. Zhang is supported in part by NSF Grants ATM-0727668 and AGS-1061998, NOAA Grant NA08OAR4310885, and NASA Grant NNX08AI74G; Chen and Wang are supported by the National Natural Science Foundation of China (40730843), the National Basic Research Program of China (2007CB816005), and International Corporation Program of China (2008DFA22230).

REFERENCES

Anderson, W. G., A. Gnanadesikan, R. Hallberg, J. Dunne, and B. L. Samuels, 2007: Impact of ocean color on the maintenance of the Pacific cold tongue. *Geophys. Res. Lett.,* **34,** L11609, doi:10.1029/2007GL030100.

Ballabrera-Poy, J., R. G. Murtugudde, J. R. Christian, and A. J. Busalacchi, 2003: Signal-to-noise ratios of observed monthly tropical ocean color. *Geophys. Res. Lett.,* **30,** 1645, doi:10.1029/2003GL016995.

——, ——, R.-H. Zhang, and A. J. Busalacchi, 2007: Coupled ocean–atmosphere response to seasonal modulation of ocean color: Impact on interannual climate simulations in the tropical Pacific. *J. Climate,* **20,** 353–374.

Barnett, T. P., M. Latif, N. Graham, M. Flugel, S. Pazan, and W. White, 1993: ENSO and ENSO-related predictability. Part I: Prediction of equatorial Pacific sea surface temperature with a hybrid coupled ocean–atmosphere model. *J. Climate,* **6,** 1545–1566.

Chang, P., L. Ji, and R. Saravanan, 2001: A hybrid coupled model study of tropical Atlantic variability. *J. Climate,* **14,** 361–390.

Chavez, F. P., P. G. Strutton, and M. McPhaden, 1998: Biological-physical coupling in the central equatorial Pacific during the onset of the 1997-98 El Niño. *Geophys. Res. Lett.,* **25,** 3543–3546.

——, ——, G. E. Friedrich, R. A. Feely, G. C. Feldman, D. G. Foley, and M. J. McPhaden, 1999: Biological and chemical response of the equatorial Pacific ocean to the 1997–98 El Niño. *Science,* **286,** 2126–2131.

Chen, D., L. M. Rothstein, and A. J. Busalacchi, 1994: A hybrid vertical mixing scheme and its application to tropical ocean models. *J. Phys. Oceanogr.,* **24,** 2156–2179.

Gnanadesikan, A., and W. G. Anderson, 2009: Ocean water clarity and the ocean general circulation in a coupled climate model. *J. Phys. Oceanogr.,* **39,** 314–332.

Jochum, M., S. Yeager, K. Lindsay, K. Moore, and R. Murtugudde, 2010: Quantification of the feedback between phytoplankton and ENSO in the Community Climate System Model. *J. Climate,* **23,** 2916–2925.

Lengaigne, M., C. Menkes, O. Aumont, T. Gorgues, L. Bopp, J.-M. André, and G. Madec, 2007: Influence of the oceanic biology on the tropical Pacific climate in a coupled general circulation model. *Climate Dyn.,* **28,** 503–516.

Lewis, M. R., M. E. Carr, G. C. Feldman, W. Esias, and C. McClain, 1990: Influence of penetrating solar radiation on the heat budget of the equatorial Pacific. *Nature,* **347,** 543–546.

Löptien, U., C. Eden, A. Timmermann, and H. Dietze, 2009: Effects of biologically induced differential heating in an eddy-permitting coupled ocean-ecosystem model. *J. Geophys. Res.,* **114,** C06011, doi:10.1029/2008JC004936.

Manizza, M., C. Le Quéré, A. J. Watson, and E. T. Buitenhuis, 2005: Bio-optical feedbacks among phytoplankton, upper ocean physics and sea-ice in a global model. *Geophys. Res. Lett.,* **32,** L05603, doi:10.1029/2004GL020778.

Marzeion, B., A. Timmermann, R. Murtugudde, and F.-F. Jin, 2005: Biophysical feedbacks in the tropical Pacific. *J. Climate,* **18,** 58–70.

McClain, C. R., M. L. Cleave, G. C. Feldman, W. W. Gregg, S. B. Hooker, and N. Kuring, 1998: Science quality SeaWiFS data for global biosphere research. *Sea Technol.,* **39,** 10–16.

Miller, A. J., and Coauthors, 2003: Potential feedbacks between Pacific Ocean ecosystems and internannual variations. *Bull. Amer. Meteor. Soc.,* **84,** 617–633.

Murtugudde, R., J. Beauchamp, C. R. McClain, M. Lewis, and A. J. Busalacchi, 2002: Effects of penetrative radiation on the upper tropical ocean circulation. *J. Climate,* **15,** 470–486.

Nakamoto, S., S. Kumar, J. Oberhuber, J. Ishizaka, K. Muneyama, and R. Frouin, 2001: Response of the equatorial Pacific to chlorophyll pigment in a mixed layer isopycnal ocean general circulation model. *Geophys. Res. Lett.,* **28,** 2021–2024.

——, and Coauthors, 2006: Potential feedback mechanism between phytoplankton and ocean circulation with oceanic radiative transfer processes influenced by phytoplankton-numerical ocean GCMs and an analytical solution. *Global Climate Change and Response of Carbon Cycle in the Equatorial Pacific and Indian Oceans and Adjacent Land Masses*, H. Kawahata and Y. Awaya, Eds., Elsevier Oceanography Series, Vol. 73, Elsevier, 255–272.

Nerem, R. S., and G. T. Mitchum, 2002: Estimates of vertical crustal motion derived from differences of TOPEX/POSEIDON and tide gauge sea level measurements. *Geophys. Res. Lett.,* **29,** 1934, doi:10.1029/2002GL015037.

North, G. R., T. L. Bell, R. F. Cahalan, and F. J. Moeng, 1982: Sampling errors in the estimation of empirical orthogonal functions. *Mon. Wea. Rev.,* **110,** 699–706.

Paulson, C. A., and J. J. Simpson, 1977: Irradiance measurements in the upper ocean. *J. Phys. Oceanogr.,* **7,** 952–956.

Reynolds, R. W., N. A. Rayner, T. M. Smith, D. C. Stokes, and W. Wang, 2002: An improved in situ and satellite SST analysis for climate. *J. Climate,* **15,** 1609–1625.

Schneider, E. K., and Z. Zhu, 1998: Sensitivity of the simulated annual cycle of sea surface temperature in the equatorial Pacific to sunlight penetration. *J. Climate,* **11,** 1932–1950.

Shell, K. M., R. Frouin, S. Nakamoto, and R. C. J. Somerville, 2003: Atmospheric response to solar radiation absorbed by phytoplankton. *J. Geophys. Res.,* **108,** 4445, doi:10.1029/2003JD003440.

Stramska, M., and D. Stramski, 2005: Effects of a nonuniform vertical profile of chlorophyll concentration on remote-sensing reflectance of the ocean. *Appl. Opt.,* **44,** 1735–1747.

Strutton, P. G., and F. P. Chavez, 2004: Biological heating in the equatorial Pacific: Observed variability and potential for real-time calculation. *J. Climate,* **17,** 1097–1109.

Sweeney, C., A. Gnanadesikan, S. M. Griffies, M. J. Harrison, A. J. Rosati, and B. L. Samuels, 2005: Impacts of shortwave penetration depth on large-scale ocean circulation and heat transport. *J. Phys. Oceanogr.,* **35,** 1103–1119.

Syu, H.-H., J. D. Neelin, and D. Gutzler, 1995: Seasonal and interannual variability in a hybrid coupled GCM. *J. Climate,* **8,** 2121–2143.

Timmermann, A., and F.-F. Jin, 2002: Phytoplankton influences on tropical climate. *Geophys. Res. Lett.,* **29,** 2104, doi:10.1029/2002GL015434.

Wetzel, P., E. Maier-Reimer, M. Botzet, J. Jungclaus, N. Keenlyside, and M. Latif, 2006: Effects of ocean biology on the penetrative radiation in a coupled climate model. *J. Climate,* **19,** 3973–3987.

Zebiak, S. E., and M. A. Cane, 1987: A model El Niño/Southern Oscillation. *Mon. Wea. Rev.,* **115,** 2262–2278.

Zhang, R.-H., and S. E. Zebiak, 2004: An embedding method for improving interannual variability simulations in a hybrid coupled model of the tropical Pacific ocean–atmosphere system. *J. Climate,* **17,** 2794–2812.

——, and A. J. Busalacchi, 2008: Rectified effects of tropical instability wave (TIW)-induced atmospheric wind feedback in the tropical Pacific. *Geophys. Res. Lett.,* **35,** L05608, doi:10.1029/2007GL033028.

——, and ——, 2009: Freshwater flux (FWF)-induced oceanic feedback in a hybrid coupled model of the tropical Pacific. *J. Climate,* **22,** 853–879.

——, L. M. Rothstein, and A. J. Busalacchi, 1998: Origin of upper-ocean warming and El Niño change on decadal scales in the tropical Pacific Ocean. *Nature,* **391,** 879–882.

——, S. E. Zebiak, R. Kleeman, and N. Keenlyside, 2005: Retrospective El Niño forecast using an improved intermediate coupled model. *Mon. Wea. Rev.,* **133,** 2777–2802.

——, A. J. Busalacchi, and R. G. Murtugudde, 2006: Improving SST anomaly simulations in a layer ocean model with an embedded entrainment temperature submodel. *J. Climate,* **19,** 4638–4663.

——, ——, and D. G. DeWitt, 2008: The roles of atmospheric stochastic forcing (SF) and oceanic entrainment temperature (T_e) in decadal modulation of ENSO. *J. Climate,* **21,** 674–704.

——, ——, X. J. Wang, J. Ballabrera-Poy, R. Murtugudde, E. C. Hackert, and D. Chen, 2009: Role of ocean biology-induced climate feedback in the modulation of El Niño-Southern Oscillation (ENSO). *Geophys. Res. Lett.,* **36,** L03608, doi:10.1029/2008GL036568.

Zheng, F., J. Zhu, and R.-H. Zhang, 2007: Impact of altimetry data on ENSO ensemble initializations and predictions. *Geophys. Res. Lett.,* **34,** L13611, doi:10.1029/2007GL030451.